JOURNAL OF CHEMICAL INFORMATION AND MODELING

Article

pubs.acs.org/jcim

Free Energy Calculations Give Insight into the Stereoselective Hydroxylation of α-Ionones by Engineered Cytochrome P450 BM3 Mutants

Stephanie B.A. de Beer,[†,‡] Harini Venkataraman,[†] Daan P. Geerke,[†] Chris Oostenbrink,*[,†,‡] and Nico P.E. Vermeulen[†]

[†]Leiden-Amsterdam Center for Drug Research, Division of Molecular and Computational Toxicology, Department of Chemistry and Pharmaceutical Sciences, Vrije Universiteit, De Boelelaan 1083, 1081 HV Amsterdam, The Netherlands

[‡]Institute of Molecular Modeling and Simulation, University of Natural Resources and Life Sciences, Muthgasse 18, A-1190, Vienna, Austria

Supporting Information

ABSTRACT: Previously, stereoselective hydroxylation of α-ionone by Cytochrome P450 BM3 mutants M01 A82W and M11 L437N was observed. While both mutants hydroxylate α-ionone in a regioselective manner at the C3 position, M01 A82W catalyzes formation of *trans*-3-OH-α-ionone products whereas M11 L437N exhibits opposite stereoselectivity, producing *trans*-(3*S*,6*S*)-OH-α-ionone and *cis*-(3*S*,6*R*)-OH-α-ionone. Here, we explore the stereoselective C3 hydroxylation of α-ionone by Cytochrome P450 BM3 mutants M01 A82W and M11 L437N using molecular dynamics-based free energy calculations to study the interaction between the enzyme and both the substrates and the products. The one-step perturbation approach is applied using an optimized reference state for substrates and products. While the free energy differences between the substrates free in solution amount to ∼0 kJ mol^{-1}, the differences in mutant M01 A82W agree with the experimentally obtained dissociation constants K_d. Moreover, a correlation with experimentally observed trends in product formation is found in both mutants. The trans isomers show the most favorable relative binding free energy in the range of all four possible hydroxylated diastereomers for mutant M01 A82W, while the trans product from (6*S*)-α-ionone and the cis product from (6*R*)-α-ionone show highest affinity for mutant M11 L437N. Marcus theory is subsequently used to relate the thermodynamic stability to transition state energies and rates of formation.

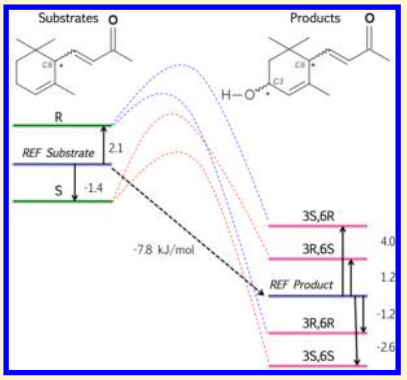

INTRODUCTION

Ionones are norisoprenoids, possessing a high aromatic potential, and therefore of great interest to the industries of aromas and fragrances.[1] Ionones feature a trimethylcyclohexane building block, which displays interesting organoleptic properties, and they are used in the preparation of perfume and flavoring compounds.[2]

The two enantiomers of α-ionone possess different odors, posing an additional challenge for the fragrance industry. For instance, (6*R*)-α-ionone is the single-enantiomeric form of α-ionone present in *Viola odorata* and typically possesses a more and stronger floral scent than (6*S*)-α-ionone, which features a cedarwood-like smell.[3,4] Furthermore, hydroxylation derivates of α-ionone are highly desirable compounds and of significant commercial interest.[3,5]

The regio- and stereoselective hydroxylation of C−H bonds poses a serious challenge to synthetic organic chemistry, due to the complexity of the reaction and the lack of overall chemo-, regio- and enantioselectivity.[6,7] Besides chemical synthesis, biosynthesis by (engineered) enzymes can form an effective and efficient alternative to generate ionone derivatives,[8] including production of 3-OH-α-ionone in a trans-oriented manner exclusively.[9]

Cytochrome P450s (CYP450) are a family of monooxygenase enzymes that facilitate important phase I metabolic processes and are known to catalyze hydroxylation of a wide range of substrates, often in a regio- and stereoselective manner.[10] It was already shown that CYP450s are versatile biocatalysts, capable of catalyzing selective oxidation of different terpenes, terpenoids, and norisoprenoids, including ionones.[11−14]

The bacterial CYP450 variant CYP102A1 from *Bacillus megaterium*, also referred to as CYP450 BM3, is well known for its high catalytic activity and solubility and is widely used in modern biotechnology.[15,16] In the past decade, numerous studies have been reported on the engineering of CYP450 BM3 as robust and useful biocatalysts for industrial applications,[17] also involving biotransformation of α-ionones and β-ionones.[18]

Previous results from our laboratory for the first time described the regio- and stereoselective hydroxylation of α-

Received: May 24, 2012
Published: July 4, 2012

ionone by CYP450 BM3.[19] CYP450 BM3 mutants M01 A82W and M11 L437N were shown to produce 3-OH-α-ionone in a stereoselective manner, with a diastereomeric excess of more than 90%. Whereas M01 A82W showed selectivity for *trans*-3-OH-α-ionone formation for both substrate enantiomers, leading to (3*R*,6*R*)-OH-α-ionone and (3*S*,6*S*)-OH-α-ionone, M11 L437N exhibited opposite stereoselectivity, producing the trans diastereomer (3*S*,6*S*)-OH-α-ionone and the cis diastereomer (3*S*,6*R*)-OH-α-ionone.[19] Figure 1 schematically depicts the stereoselective hydroxylation by the CYP450 BM3 mutants as well as the structures of the diastereomers.

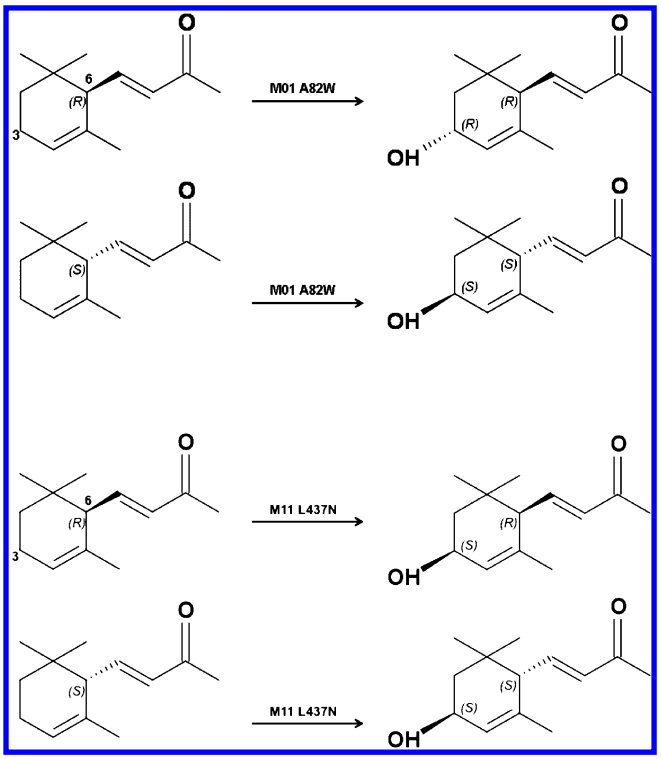

Figure 1. Structures of (*R*)- and (*S*)-α-ionone enantiomers and their three hydroxylated products by CYP450 BM3 mutants M01 A82W and M11 L437N, adapted from ref 19. (3*R*,6*R*)-OH-α-ionone and (3*S*,6*S*)-OH-α-ionone are trans isomers, whereas (3*S*,6*R*)-OH-α-ionone is a cis isomer.

Computational approaches often can provide insights at an atomic level, typically inaccessible by experiments. Molecular docking algorithms are widely used to determine binding modes of small ligands to a biomolecular receptor and estimate a corresponding score which is related to the binding affinity toward the target.

Previous molecular docking studies on the CYP450 BM3 mutants complexes with α-ionone have given some useful structural insights into the orientations of the obtained ligands in the protein binding cavity, partially rationalizing the experimentally observed stereoselectivity.[19] However, in general, docking methods fail to accurately predict and rank binding affinities due to poor and incomplete scoring functions.[20,21]

Here, we investigate the transformation of α-ionone by CYP450 BM3 mutants in terms of the thermodynamic stability of the substrates and products within the active sites. Although this requires more computational effort than docking studies, the results are more reliable due to the correct representation of the system's biophysical properties through the use of an accurate force field and sufficient conformational sampling.

Accurate calculations of substrate and product binding affinities can give direct insights into the stereoselectivity of hydroxylation by CYP450 BM3 because differences in the intrinsic reactivity of C−H bonds at the same carbon center (C3) will be small.

Prediction of the binding affinity of a ligand binding to a receptor is one of the most important challenges in modern-day computational chemistry. An accurate and reliable prediction of binding affinities of (small) ligands to biomolecular targets requires a precise assessment of their binding free energies, an important thermodynamic quantity, readily defined from statistical mechanics.[22]

Various approaches exist to estimate binding affinity from molecular simulations and exact statistical thermodynamics, the most efficient still seeming to be estimation of relative free energies for different thermodynamic states[23,24] through the definition of a suitable thermodynamic cycle.[25,26] The most well-known method connecting the thermodynamic states in such a cycle is free energy perturbation (FEP),[27,28] which is applied in the one-step perturbation (OSP).[29,30] Another widely used method is thermodynamic integration (TI).[31]

The difficulty in calculating the free energy difference between two thermodynamic states, A and B, arises from the fact that the distribution of relevant configurations for states A and B may well be too different to show overlap in an ensemble average. In order to connect the two states and calculate the free energy difference between them, one typically defines a series of (unphysical) intermediate states, between which the conformational ensembles overlap. In TI state A is gradually changed into state B in a number of discrete steps of unphysical intermediates. In OSP, a reference state is defined which is represented by a single, broad ensemble for which overlap with the ensembles of both states A and B is possible. Moreover, the reference state (not necessarily being physical) can be designed such that overlap with the ensembles of multiple end states is possible as long as it samples a sufficient amount of conformations that are relevant for the real states individually. Therefore, whereas TI is computationally expensive and can only take a few compounds into account in a highly accurate manner, OSP may be more efficient as it can estimate free energies for more compounds from a single simulation.

In this study, we explore the stereoselective C3 hydroxylation of α-ionone by CYP450 BM3 mutants M01 A82W and M11 L437N by calculating the relative stabilities of the various stereoisoemeric substrates and products using the TI and OSP methods.

For this purpose, a substrate reference state was designed and optimized based on OSP simulations of α-ionone free in aqueous solution, after which results were compared to TI calculations. Subsequently, the optimized reference state and a derived reference state for the product diastereomers were used to calculate differences in binding free energies for the substrates and products, respectively. In this way, a correlation with experimental trends in preferred binding and product formation was obtained.

METHODS

Thermodynamic Integration. TI makes use of the coupling parameter approach to alchemically connect the two Hamiltonians describing two states A and B over a path defined by λ. At $\lambda = 0$, the Hamiltonian $H(\lambda)$ describes state A, and at λ

= 1, it represents state B. At intermediate λ values the exact functional form of H represents a possibly unphysical intermediate.[32]

The free energy difference ΔG_{AB} between the two states can be calculated by numerical integration of the λ derivative of H along this path according to eq 1[28]

$$\Delta G_{AB} = \int_0^1 \left\langle \frac{\partial H(\lambda)}{\partial \lambda} \right\rangle_\lambda d\lambda \quad (1)$$

where the angular brackets denote the ensemble average of the derivative of H with respect to λ, which is obtained from independent simulations at discrete intermediate values of λ.

In this study, we applied TI to calculate the free energy difference accompanying inversion of the stereocenter of α-ionone free in aqueous solution, represented by $\Delta G_{AB} = \Delta G_{inv}^{free}$ in a two-step process. This approach was previously shown to be more efficient than a dual-topology approach in which functional groups are removed and added at stereospecific locations.[33] First, one enantiomer, (6*R*)-α-ionone, was modified into a planar intermediate state, *I*, in 11 independent simulation steps defined by 11 equidistant values of λ to generate the ensemble average in eq 1. State *I* differs from the end states in the definition of the zero-energy value of the improper dihedral angle (0° rather than ~35° and ~325° for (6*R*)- and (6*S*)-α-ionone, respectively) and of the bond angles (120° rather than 109.5°) around the C6 stereocenter.

The intermediate state was subsequently modified into the other enantiomer, (6*S*)-α-ionone, using again 11 independent simulation steps. In order to monitor convergence, the free energy difference corresponding to the backward processes was also calculated by performing the (6*S*) → *I* → (6*R*)-inversion in a similar way. The difference between estimates from the forward and backward simulations defines the hysteresis, which should be zero exactly. Because ΔG_{inv}^{free} for enantiomers should equal zero, the convergence (and accuracy) of the TI calculations is also tested by the criterion that the calculated free energy difference is sufficiently close to 0.

One-Step Perturbation. The OSP method is directly derived from the FEP formula 2,[27] where the difference between a reference state (REF, or R) and real state (A) can be directly calculated from the simulation trajectories of the reference state

$$\Delta G_{RA} = -k_B T \ln\langle e^{-(H_A - H_R)/k_B T}\rangle_R \quad (2)$$

In eq 2 the angular brackets denote the ensemble average over all configurations of the reference state generated in a MD simulation, k_B is the Boltzmann constant, T is the temperature, and H_A and H_R are the Hamiltonians of the system for states A and R, respectively, calculated for the configurations sampled for the reference state. Free energy differences ΔG_{RB}, ΔG_{RC}, ... between states B, C, ... and R can also be calculated by substituting A in eq 2 with B, C, ... The relative binding free energy between real states A and B can subsequently be obtained from

$$\Delta G_{AB} = \Delta G_{RB} - \Delta G_{RA} \quad (3)$$

One of the most crucial steps when applying the OSP method successfully is the choice of the reference state.[34] In this study, however, choosing an initial reference state (N) was relatively straightforward. For substrates (6*R*)- and (6*S*)-α-ionone N was defined by setting the force constant for the improper dihedral term for the stereocenter (atom C6) to zero, thereby facilitating the reference state to make transitions between the two enantiomeric states (switching of the 'tail' moiety). For the products, the reference state was expanded by addition of a hydroxyl moiety on C3, creating a second stereocenter, and subsequently removing the improper dihedral interaction on that stereocenter (Figure 2). This allows the product reference state to sample the four enantio- and diastereomeric products, (3*S*,6*R*)-, (3*S*,6*S*)-, (3*R*,6*S*)-, and (3*R*,6*R*)-OH-α-ionone.

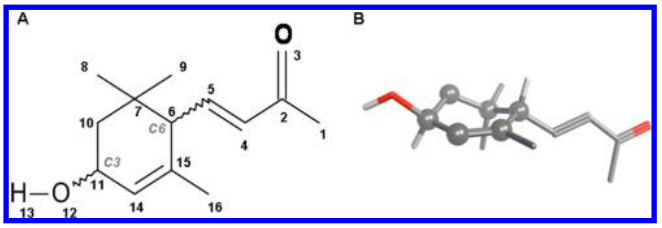

Figure 2. Depiction of the reference state, R, as used in one-step perturbation simulations for the products (A). In the substrate simulations, a similar reference state is used, with O12 and H13 being replaced with a hydrogen atom at position 12. Atom numbers are used to define the force field parameters in the Supporting Information. Indices C3 and C6 refer to the stereocenters in the product. (B) 3D representation of (3*S*,6*S*)-OH-ionone is depicted.

As mentioned previously, simulation of the reference state should sample as many conformations of the real states as possible. However, in initial simulations of the substrate reference state the switching between the α-ionone enantiomers was far from sufficient (see Results and Discussion section). Hence, the representation of the substrate's reference state in the simulation free in solution was optimized such that a significant number of transitions between the (6*R*)- and the (6*S*)-configuration was observed. For this purpose, bonded as well as nonbonded interaction terms in the reference Hamiltonian were adapted in order to lower energetic barriers separating both states. Close inspection of the torsional dihedral angle interactions along the ring system indicated, e.g., that the ring is rather rigid and must undergo a conformational change in order for the molecule to turn over from its (6*R*)- to the (6*S*)-configuration and vice versa.

In total, five reference state models were generated based on four modifications to N (the letters A, P, D, and E are used in Table 1 to refer to the various modifications).

A: Bond angle bending force constant (k_θ) for the bond angles around C6 was lowered from 520 to 285 kJ mol^{-1}.
P: Proper dihedral angle force constant (k_ϕ) for the torsional dihedral angle around the C5−C6 bond was lowered from 3.77 to 1.0 kJ mol^{-1}.
D: Proper dihedral angle force constants (k_ϕ) for the ring torsional dihedral angles were lowered from 5.86 to 1.26 kJ mol^{-1}.
E: C8, C9, and C16 are taken up in the nonbonded exclusion list for C5.

Note that these modifications only involve the reference state and correspondingly H_R in eq 2 but not the real compounds (6*R*)-α-ionone (H_A) and (6*S*)-α-ionone (H_B).

Simulation Settings. All molecular dynamics simulations were performed using the GROMOS11 biomolecular simulation package.[32,35] Interaction parameters to describe the ligands and proteins were taken from the GROMOS parameter

Table 1. Calculated Free Energy Difference ΔG_{RS} (in kJ/mol) between Hydrated (6*S*)-α-Ionone and (6*R*)-α-Ionone, As Obtained from TI and OSP Calculations of α-Ionone Free in Solution[a]

TI	description I		$\Delta G_{R\to I}$	$\Delta G_{I\to S}$	ΔG_{RS}
	unmodified	forward	−17.5 ± 0.9	30.7 ± 1.8	13.2
		backward	33.5 ± 1.0	−27.4 ± 0.9	6.1
	+ modifications	forward	−23.4 ± 0.7	23.9 ± 1.1	0.5
	A + P + D + E	backward	23.5 ± 1.1	−23.5 ± 0.7	0.0
OSP	reference state used	starting configuration substrate	$\Delta G_{REF\to R}$	$\Delta G_{REF\to S}$	ΔG_{RS}
1	N	6*R*	6.5	12.0	5.5
2	N + A + P	6*R*	15.3	26.4	11.1
		6*S*	15.2	21.4	6.2
3	N + A + P + E	6*R*	19.9	25.2	5.3
		6*S*	21.2	21.5	0.3
4	N + A + P + D	6*R*	22.9	23.9	1.0
		6*S*	23.4	23.3	−0.1
5	N + A + P + D + E	6*R*	30.6	30.3	−0.3
		6*S*	30.2	30.1	−0.1

[a]Properties that are altered in the representation of *I* and of the OSP reference state are described in the Methods section and are named as follows: N = normal OSP reference state; removed improper dihedral interaction term on C6, A = reduced force constants for the bond angles around the C6 stereocenter, P = reduced force constant for the proper dihedral angle around the C5−C6 bond, D = reduced force constants for the ring torsional dihedrals, E = excluding selected (1,4)-interactions for C5 from the nonbonded interactions.

set 45A4[36] and are available in the Supporting Information (ligands).

OSP simulations were performed for the unphysical reference states representing α-ionone substrates and products, both in aqueous solution, and bound to proteins CYP450 BM3 M01 A82W and M11 L437N.

TI simulations were carried out for the substrates free in aqueous solution only. For one alchemical transformation, 11 λ values were used. After an equilibration time of 50 ps, simulations of 1 ns were performed at every λ value, such that the total path of a stereocenter inversion was 22 ns long.

Starting coordinates for the (6*R*)- and (6*S*)-α-ionone substrate reference state in complex with mutants M01 A82W and M11 L437N were selected from previous docking studies,[19] to which a hydroxyl moiety was added manually to obtain starting coordinates for simulations of the 3-OH-α-ionone product reference state, using the molecular builder tool as implemented in MOE (Molecular Operating Environment).[37] Note that the initial poses are in line with the experimentally observed site of metabolism at C3.[19]

In order to monitor convergence and increase sampling, simulations of the reference states in water and in the proteins were started from two different starting configurations (corresponding to a (6*R*)- and a (6*S*)-α-ionone conformation, respectively). Figure 3A shows the two starting configurations for the substrate's reference state in M01 A82W. For simulations of the product's reference state in protein M01 A82W, three different starting configurations were used, one corresponding to the (3*R*,6*R*)-configuration and two corresponding to the (3*S*,6*S*)-configuration.

The ligands and protein−ligand complexes were solvated in periodic rectangular boxes, containing ∼2000 and ∼17 000 SPC water molecules,[38] respectively, using a minimum solute to wall distance of 0.9 nm. The solvated protein−ligand complexes contained 15 or 13 Na^+ ions to neutralize the system for M01 A82W and M11 L437N, respectively.

In all MD simulations, a time step of 2 fs was used. In an equilibration phase, the system was gradually heated up to 298 K in three (water) and seven (protein) separate simulation steps of 20 ps each. In the first five protein equilibration steps position restraints were applied to the protein and reference state atoms using a gradually decreasing force constant (starting from 2.5×10^4 kJ mol^{-1} nm^{-2}). After the equilibration phase, a production MD simulation at 298 K of 10 or 20 ns followed, during which no position restraints were applied. Covalent bonds were kept constrained using the SHAKE algorithm,[39] with a relative tolerance of 10^{-4}. During the production simulations the temperature was kept constant (298 K) as well as the pressure (1 atm) using the weak coupling algorithm[40] with a coupling time of 0.1 and 0.5 ps, respectively. The isothermal compressibility was set to 4.575×10^{-4} (kJ mol^{-1} $nm^{-3})^{-1}$.

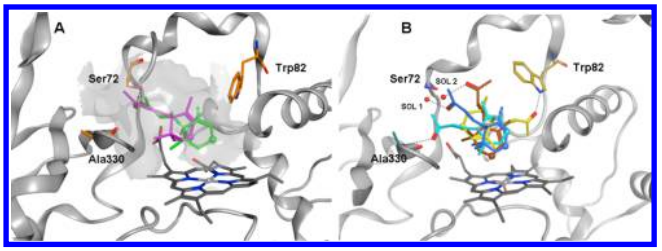

Figure 3. α-Ionone orientations in the active site of the heme domain of cytochrome P450 BM3 mutant M01 A82W. Side chains of selected amino acid residues, the catalytically active heme group, and α-ionone are depicted in stick representation. Black thin lines represent hydrogen bonds formed between the carbonyl oxygen of α-ionone and either Ser72 (A), Trp82, Ala330, or solvent molecules (B). (A) Starting structures are shown for the MD simulations of the substrate reference state in the OSP approach, starting from (6*R*)- and (6*S*)-configurations of α-ionone (depicted in green and magenta sticks, respectively). (B) Most abundant α-ionone orientations observed during both MD simulations, obtained from a combined cluster analysis of the two runs. Central members of the four largest clusters are depicted in dark blue (cluster 1), brown (cluster 2), cyan (cluster 3), and yellow (cluster 4) stick representation. See Figure 9 for the distribution of the clusters and their corresponding percentages of contribution with respect to the total number of structures.

At every time step nonbonded interactions were calculated up to a distance of 0.8 nm by means of a pairlist that was generated every five steps. At every fifth time step, intermediate-range interactions at distances up to 1.4 nm were calculated and kept constant between updates. To account for electrostatic interactions beyond the cutoff radius of 1.4 nm, a reaction-field contribution was added to the energies and forces,[41] with a dielectric permittivity of 61.[42] During the production simulations, coordinates were stored every 100 (0.2 ps) and 250 (0.5 ps) steps for water and protein, respectively.

RESULTS AND DISCUSSION

Thermodynamic Integration Free in Solution. The values of $\langle \partial H/\partial\lambda \rangle_\lambda$ as a function of λ for the two-step TI process are shown in Figure 4. Note that for $\lambda = 1$ in $R \rightarrow I$ and

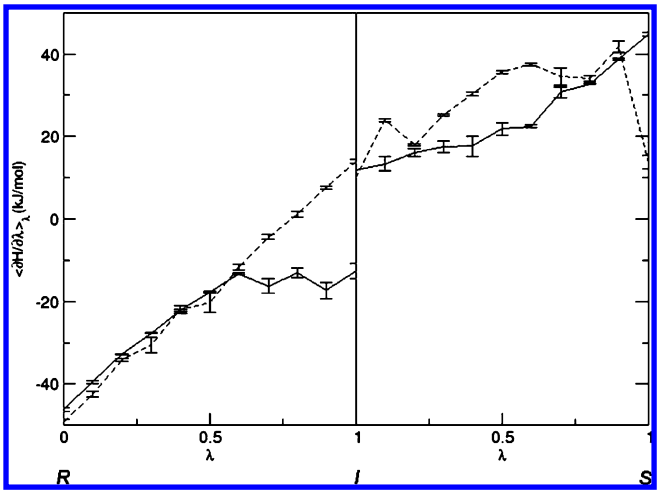

Figure 4. Values of $\langle \partial H/\partial\lambda \rangle_\lambda$ as a function of λ for the two-step TI perturbation process for calculation of ΔG_{inv}^{free}. (Left) Forward transformation for (6*R*)-α-ionone into intermediate state *I*. (Right) Forward transformation for *I* into (6*S*)-α-ionone. Both the optimized and the original models of *I* are displayed in solid and dotted lines, respectively (see the Methods section for further details of the two representations of *I*).

$\lambda = 0$ in $I \rightarrow S$, different $\langle \partial H/\partial\lambda \rangle_\lambda$ values can be obtained, since the modification of the angles around C6 is reverted from $R \rightarrow I \rightarrow S$ (109.5° → 120° → 109.5°), while the improper dihedral angle is inverted (+35.26° → 0° → −35.26°). Forward and backward values of the relative binding free energies as estimated from the obtained TI profiles between the (6*R*)- and (6*S*)-α-ionone substrates and the intermediate state, *I*, are shown in Table 1.

Since (6*R*)- and (6*S*)-α-ionone are enantiomers, the free energy difference between these two compounds in solution should be zero. However, for the results obtained with initial TI calculations this is not the case, the sum being 13.2 kJ mol^{-1} (see Table 1, upper part). Furthermore, the hystereses amount to 3.3−16.0 kJ mol^{-1}.

When similar alchemical transformations were performed, but using a newly defined intermediate state in which modifications A, P, D, and E as described for the OSP reference state were included, no hysteresis was observed and the sum of $R \rightarrow I$ and $I \rightarrow S$ was virtually zero (A + P + D + E in Table 1, upper part).

One-Step Perturbation Free in Solution. To optimize the reference state, five different substrate reference states were used in OSP simulations in water, for which the calculated free energy differences are shown in the lower part of Table 1. For reference state models 2−5 values are given for two (independent) simulations, starting from either an (*R*)- or a (*S*)-configuration. Since (6*R*)- and (6*S*)-α-ionone are enantiomers, the free energy difference between these two states should amount to zero in achiral environment. As shown in Table 1, the optimized model 5 shows $\Delta G_{RS} \approx 0$ kJ mol^{-1} as well as convergence between the two independent simulations.

Figure 5 presents time series of the improper dihedral angle on the C6 stereocenter in simulations of the substrate's

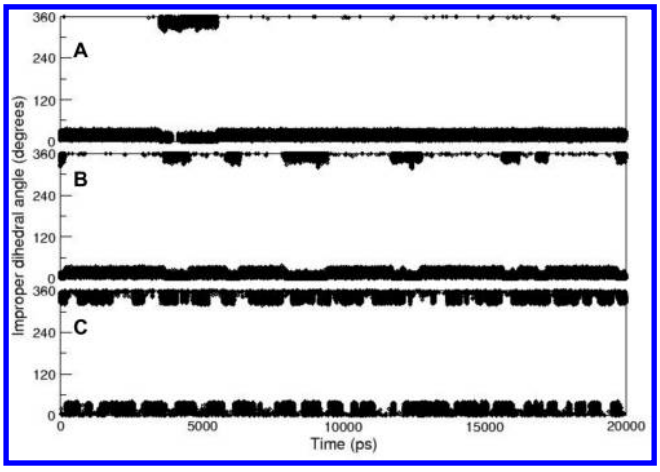

Figure 5. Time series of the improper dihedral angle value for the α-ionone C6-stereocenter, as calculated from 20 ns MD simulations of the substrate reference state free in solution. Depicted are reference state models N (A), N + A + P (B), and N + A + P + D + E (C), starting from an initial (6*R*-), (6*S*-), and (6*S*)-configuration of the substrate, respectively. For classifications of the various models see the Methods section. The improper dihedral at C6 adopts value of ∼35° and ∼325° corresponding to (6*R*)- and (6*S*)-α-ionone, respectively.

reference state free in solution for three different models. Figure 5A depicts results obtained for the initial model N and merely shows a single transition from the (6*R*)- to the (6*S*)-configuration during the simulation. For N, the reference state simulation is not converged, which is reflected by the significant value for the calculated free energy difference of $\Delta G_{RS} = 5.5$ kJ mol^{-1} (Table 1). In Figure 5B, results from simulations using model N + A + P is shown, where alterations have been made to the representation of the C6 stereocenter. The force constants of the bond angles around C6 and the dihedral angle over the bond C5−C6 have been lowered, lowering energetic barriers separating the (6*S*)- and the (6*R*)-conformation and allowing for a smoother inversion of the C6 stereocenter. Indeed, more transitions are observed in Figure 5B. However, the transitions are still too rare, considering the corresponding free energy differences in Table 1. No convergence is observed between the two independent simulations with $\Delta G_{RS} = 11.1$ and 6.2 kJ mol^{-1}, respectively. However, Figure 5C shows that the optimized reference state model N + A + P + D + E allows for many fast and reversible inversions of the C6 stereocenter. The time series of the torsional dihedral angles within the ring system support the fact that the ring adopts different conformations when in the (6*R*)- or (6*S*)-configuration (data not shown). Therefore, lower ring dihedral angle force constants are necessary in order to enhance these conformational changes in the OSP substrate reference state simulations

dx.doi.org/10.1021/ci300243n | J. Chem. Inf. Model. 2012, 52, 2139−2148

(model N + A + P + D). Additionally, excluding the nonbonded interactions of (1,4) neighbors of C5 (modification E) further increases the number of transitions between the (6*S*)- and the (6*R*)-configuration (Figure 5C).

Comparison of TI and OSP. When calculating free energies of binding with the various available computational approaches there is always a balance between the accuracy and the reliability of such calculations on one hand and computational costs on the other. As mentioned before, molecular docking algorithms are very well applicable to predict ligand orientations in static proteins but are not the method of choice to accurately rank the corresponding binding affinities.[20,21] Although TI is generally considered to be one of the most accurate methods to calculate free energy differences, it is computationally expensive.

The initial TI calculations on the transformation of the system from (6*R*)- to (6*S*)-α-ionone via an intermediate state showed no convergence. High energy barriers prohibited a necessary conformational change of the relatively rigid ring. Instead of being planar, the value for the improper dihedral angle around C6 in the intermediate state remained close to the values corresponding to either a (6*R*)- or a (6*S*)-conformation (data not shown).

A strength of OSP is that a single MD simulation of the reference state is sufficient to estimate relative binding free energies for a series of (structurally similar) compounds. In this work, one simulation of a reference state leads to two and four free energy estimates for α-ionone substrates and their hydroxylated products, respectively (see below). Moreover, the conformational changes of the ring system were easily accounted for in the optimized reference state, allowing for a more frequent transition between the (6*R*)- and the (6*S*)-configuration (Figure 5C). Retrospectively using the optimized force-field parameters for definition of the intermediate state in the TI calculations free in solution also yielded well-converged results.

Interestingly, in this study we show that TI is not necessarily the most reliable method but that similar or even more accurate results can be obtained when applying the less expensive OSP method on the very same system.

One-Step Perturbation Bound to the Protein. In a next step, simulations of the substrate and product reference states N + A + P + D + E bound to the protein were performed. To test the stability of the protein structures throughout the simulations, the atom-positional root-mean-square deviations (rmsd) of the backbone heavy atoms with respect to the initial structure were calculated. These remained stable, with maximum values of ca. 0.37 and 0.30 nm for mutant M01 A82W and M11 L437N, respectively.

Figures 6 and 7 show the time series of the improper dihedral angle value for the α-ionone stereocenters throughout the 20 ns simulations of the substrate (Figure 6A) and the product (Figure 6B–D) reference states in M01 A82W and throughout the 10 ns simulations of the substrate (Figure 7A) and product (Figure 7B and 7C) reference states in M11 L437N. Independent simulations were performed, starting from different configurations of the ligand in the protein active site. The free energy differences of the *N* individual simulations were combined using their Boltzmann-weighted averages according to

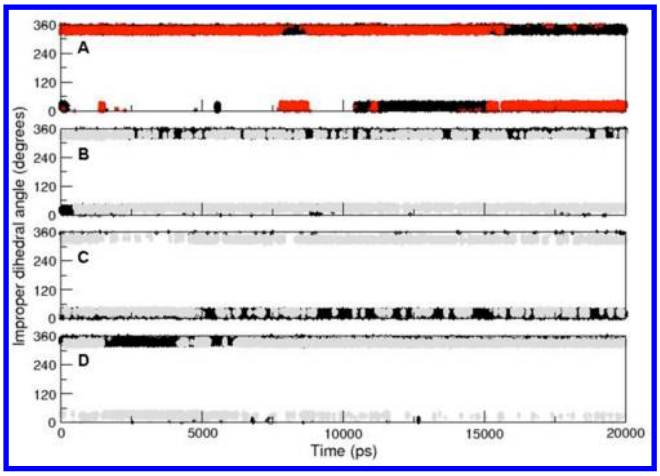

Figure 6. Time series of the improper dihedral angle value for the α-ionone stereocenter(s), as calculated from 20 ns MD simulations of CYP450 BM3 mutant M01 A82W in complex with the reference state N + A + P + D + E for both α-ionone substrate (A) and product (B–D) calculations. (A) Two independent simulations of the substrate reference state, starting from different starting configurations (black and red). (B, C, and D) For three independent simulations (starting from different starting configurations of the ligand) the improper dihedral angle values for the 3-OH-α-ionone C3 (gray) and C6 (black) stereocenters. The improper dihedral at C6 adopts values of ∼35° and ∼325° in (6*R*)- and (6*S*)-α-ionone, respectively, and the improper dihedral at C3 adopts values of ∼35° and ∼325° in (3*S*)- and (3*R*)-OH-α-ionone, respectively.

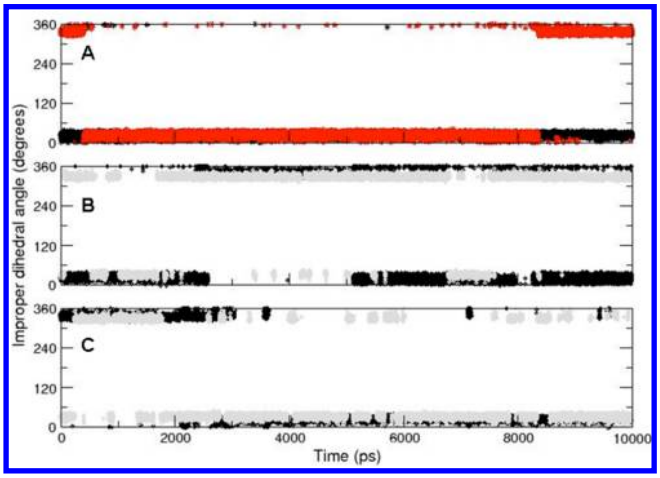

Figure 7. Time series of the improper dihedral angle value for the α-ionone stereocenter(s), as calculated from 10 ns MD simulations of CYP450 BM3 mutant M11 L437N in complex with the reference state, for both α-ionone substrate (A) and product (B and C) calculations. (A) Two independent simulations of the substrate reference state, starting from different starting configurations (black and red). (B and C) For two independent simulations (starting from different starting configurations of the ligand) the improper dihedral angle values for the 3-OH-α-ionone C3 (gray) and C6 (black) stereocenters. The improper dihedral at C6 adopts values of ∼35° and ∼325° in (6*R*)- and (6*S*)-α-ionone, respectively, and the improper dihedral at C3 adopts values of ∼35° and ∼325° in (3*S*)- and (3*R*)-OH-α-ionone, respectively.

$$\Delta G_{\mathrm{comb}} = -k_{\mathrm{B}}T \ln\left[\frac{1}{N}\left(\sum_{n=1}^{N} e^{(-\Delta G_n/k_{\mathrm{B}}T)}\right)\right] \quad (4)$$

dx.doi.org/10.1021/ci300243n | J. Chem. Inf. Model. 2012, 52, 2139–2148

Equation 4 is reminiscent of the Jarzynski equation for multiple nonequilibrium free energy estimates[43] and in the context of the one-step perturbation refers to the pooling of multiple simulations.[44,45] Applying the same Boltzmann averaging to the free energy differences as obtained from the reference states free in solution (shown in Table 1 for the substrates) yields the free energy differences in Table 2 from

Table 2. Comparison of Experimentally Determined Free Energies of Binding $\Delta G_{bind,exp}$ for (*R*)- and (*S*)-α-Ionone (substrates) to Values Obtained from the Differences in Free Energy ΔG between Reference and End States, Calculated from Water (free) and Protein Ensembles Generated in the One-Step Perturbation Approach Using the N + A + P + D + E Model[a]

	free	protein		
	ΔG	ΔG	ΔG_{bind}	$\Delta G_{bind,exp}$
		substrates		
		M01 A82W		
REF → *R*	30.4	32.5	2.1	3.3[b]
REF → *S*	30.2	28.8	−1.4	−1.7[b]
$\Delta\Delta G_{bind}$			−3.5	−5.0
		M11 L437N		
REF → *R*	29.9	29.5	−0.4	4.9[b]
REF → *S*	30.5	36.0	5.5	5.0[b]
$\Delta\Delta G_{bind}$			5.9	0.1
		products		
		M01 A82W		
REF → (3*R*,6*S*)	40.3	41.5	1.2	
REF → (3*S*,6*S*)	34.0	31.4	−2.6	
REF → (3*S*,6*R*)	40.4	44.4	4.0	
REF → (3*R*,6*R*)	33.8	32.6	−1.2	
		M11 L437N		
REF → (3*R*,6*S*)	39.9	43.8	3.9	
REF → (3*S*,6*S*)	33.9	32.9	−1.0	
REF → (3*S*,6*R*)	41.8	41.0	−0.8	
REF → (3*R*,6*R*)	33.7	35.4	1.7	

[a]Water and protein MD simulations for M01 A82W and M11 L437N were 20 and 10 ns long, respectively. Estimated binding free energies for 3-hydroxylated (*R*)- and (*S*)-α-ionone products are also shown. All free energy differences are given in kJ/mol. [b]Calculated from the experimentally determined dissociation constant K_d (ref 19).

which the relative binding free energies for the substrates and products can be estimated. E.g., combining the two (N = 2) independent values for $\Delta G_{REF\rightarrow R}$ for N + A + P + D + E, 30.6 and 30.2 kJ/mol (Table 1), leads to a Boltzmann-weighted average value of 30.4 kJ/mol (Table 2) according to eq 4.

Also indicated in Table 2 are the experimentally determined affinities for (6*R*)- and (6*S*)-α-ionone binding to mutants M01 A82W and M11 L437N. The dissociation constants K_d are reported in ref 19 and converted into the experimental estimate for the binding free energy, $\Delta G_{bind,exp}$, using

$$\Delta G_{bind,exp} = k_B T \ln K_d \quad (5)$$

As can be derived from Table 2, the calculated relative binding free energies are in excellent agreement with the experimentally measured affinities for M01 A82W (with a $\Delta\Delta G_{bind}$ discrepancy of 1.5 kJ mol^{-1}) as well as the overall observation that (6*S*)-α-ionone binds tighter to M01 A82W than (6*R*)-α-ionone. For M11 L437N, the calculated values deviate from the experimental data. While experiments show that there is no significant difference in affinity for (6*R*)- and (6*S*)-α-ionone, our calculations yield $\Delta\Delta G_{bind}$ = 5.9 kJ mol^{-1}. This is also reflected in Figure 7A, in which the (6*R*)-configuration is seen almost exclusively in the simulations. Because very little transitions are observed in these simulations, the calculated $\Delta\Delta G_{bind}$ are not converged and cannot be trusted.

Subsequently, binding free energies for all four possible 3-OH-α-ionone products, (3*R*,6*S*)-, (3*S*,6*S*)-, (3*S*,6*R*)-, and (3*R*,6*R*)-OH-α-ionone, were calculated (Table 2). Interestingly, the values of the products free in solution indicate an intrinsically preferred trans orientation for substrate hydroxylation, since these values are lower in free energy than the values for the diastereomeric cis-oriented hydroxylation. As shown in Figure 1, this intrinsic trans preference for 3-OH-α-ionone hydroxylation is enhanced in mutant M01 A82W but inverted for the (6*R*)-substrate in M11 L437N.

The computed binding affinities for the 3-OH-α-ionone products to the mutants correlate with the experimentally determined product formation. The products of α-ionone which are lowest in binding free energy, $\Delta G_{bind,calc}$, are the products of (6*R*)- and (6*S*)-α-ionone that are being formed, as can be derived by comparing the values in Table 2 to the product formation in Figure 1.

For M01 A82W, the (3*R*,6*R*)-product is lower in free energy than the (3*S*,6*R*)-product (by 5.2 kJ mol^{-1}) and (3*S*,6*S*) is lower in free energy than (3*R*,6*S*) (by 3.8 kJ mol^{-1}), predicting trans hydroxylation. Another observation is that these products are lower in binding free energy than their reference state compound. This is graphically depicted in Figure 8, which gives a schematic representation of all obtained values for ΔG_{bind} for α-ionone substrates and products to M01 A82W. The free energy difference between the reference states for the substrates and for the products was obtained from a OSP calculation (eq 2) over the product reference state using for the real state a Hamiltonian H_A in which the 3-OH group is modified into a hydrogen atom. Note that the observation that all four products in Figure 8 are lower in binding free energy than the substrates could hint at product inhibition, not uncommon for BM3 reactions (private communication).

According to Marcus theory,[46] the thermodynamic stability of the trans products also suggests a lower transition state for the corresponding reactions and hence an increased rate of trans product formation. This is graphically depicted in Figure 8 by the dotted lines connecting the substrates and the products.

For M11 L437N, a different trend is predicted with (3*S*,6*R*)-OH-α-ionone having a lower binding free energy with respect to the reference state than (3*R*,6*R*)-OH-α-ionone with a difference of 2.5 kJ mol^{-1}. This implies that for (6*R*)-α-ionone, cis hydroxylation is preferred. For (6*S*)-α-ionone, opposite stereoselectivity is predicted, since the (3*S*,6*S*)-product is lower in binding free energy than the (3*R*,6*S*)-product, by 4.9 kJ mol^{-1}. Again, this correlates with the experimentally observed trends (Figure 1).

Conformational Sampling. To investigate the conformational sampling of the protein−ligand complexes in the generated ensembles, cluster analyses were performed after combining the various independent simulations that started from different starting configurations of the product or substrate reference state. For all pairs of stored configurations, the root-mean-square difference of atomic positions of the ligand was calculated after a rotational fit based on the positions of the backbone heavy atoms of the protein. Structural neighbors were determined using a cutoff rmsd value of 0.15

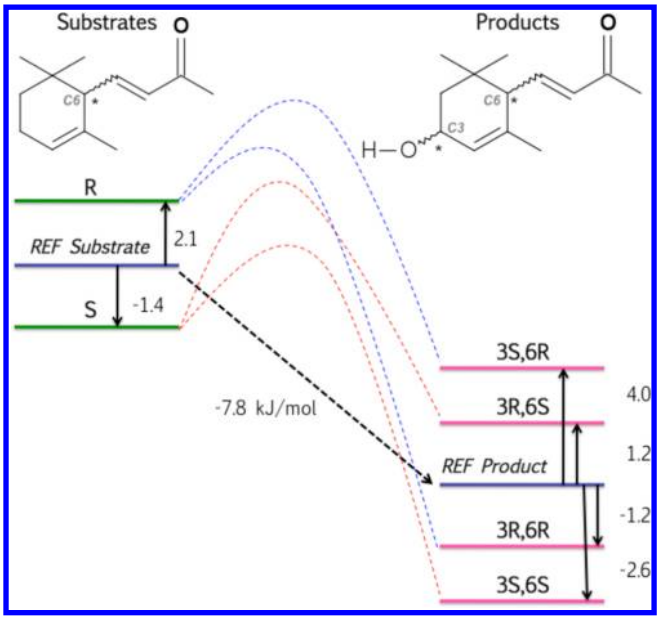

Figure 8. Overview of estimated relative binding free energies (ΔG_{bind} in Table 2) from the OSP calculations for α-ionone in complex with CYP450 BM3 mutant M01 A82W. (Top left side) Structure of the substrate reference state is shown; the C6 stereocenter is indicated with an asterisk. Calculated values for the binding free energies of α-ionone substrates to M01 A82W are given on the left side, relative to the substrate reference state. (Top right side) Structure of the product reference state is shown; both C3 and C6 stereocenters are indicated with an asterisk. Values for the binding of OH-α-ionone products to M01 A82W are given on the right side, relative to the product reference state. Dotted lines connecting end states represent reaction pathways, including transition states. Blue and red reaction pathways are associated with (6*R*)- or (6*S*)-α-ionone, respectively. Dashed black line indicates the calculated difference in free energy between the two employed reference states.

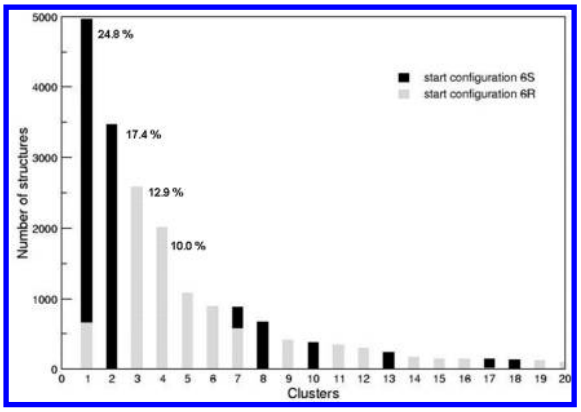

Figure 9. Cluster analysis of α-ionone conformations observed in the combined ensembles generated in the two independent MD simulations, starting from different configurations of the substrate reference state in BM3 mutant M01 A82W. Total amount of structures included in the cluster analysis is 20 000. Number of structures in the 20 largest clusters is indicated, where black bars correspond to structures originating from the simulation starting in the (6*S*)-configuration and gray bars to structures from the simulation starting in the (6*R*)-configuration.

nm, and clusters of similar conformations were obtained as described earlier.[47]

For the substrate reference state in complex with M01 A82W, the populations of the 20 largest structural clusters are shown in Figure 9. The two independent simulations starting from different starting configurations of the substrate were combined, allowing for an assessment of the sampling of the adopted binding orientations during both simulations. Structures from both simulations were found to contribute to the largest cluster (24.8% of the total number of structures), confirming that the most abundant conformation of the ligand is present in the two simulations. However, this is the only cluster in which substantial overlap is observed. Although cluster number 7 is also sampled in both simulations, the number of structures contributing to this cluster compared to the total number of structures is relatively low (4.4%).

In Figure 3B, the orientations of the central member structures of the four largest clusters for the substrate reference state bound to M01 A82W are depicted. The conformations are quite different (indicating proper sampling of the substrate within the active site) not only in terms of their distinct orientations in the binding cavity but also in terms of the specific interaction patterns with active site amino acid residues or solvent molecules. Interestingly, the central member of the first cluster is oriented in the protein cavity such that formation of a hydrogen bond with Ser 72 is possible. This is in line with previous docking results, where hydrogen-bond formation with this particular residue was observed for docked poses of α-ionone in the M01 A82W protein active site.[19]

For the other complexes, the multiple simulations starting from different reference state configurations showed virtually no overlap between the generated ensembles in terms of their contribution to the obtained clusters (data not shown). The lack of structural overlap between the generated ensembles can also be seen from Figures 6 and 7. The black circles in Figure 6B–D show that in the three simulations of the product reference state in M01 A82W the tail moiety of the ligand is fixed in a (6*R*)- (Figure 6C) or (6*S*)-conformation (Figure 6B and 6D). In Figure 7, only a few stereoinversions at C6 are observed in the substrate (Figure 7A) and product reference state (Figure 7B and 7C) simulations in M11 L437N. In all product simulations, the second stereocenter (C3, gray circles in Figures 6 and 7) shows sufficient transitions such that the attached hydroxyl moiety samples both states, allowing for a reasonable estimate of the preference between the cis and the trans products of both (6*R*)- and (6*S*)-α-ionone.

The limited structural overlap between the ensembles generated in the simulations started from different reference state configurations emphasizes the importance of averaging individual runs using eq 4. Only through the Boltzmann-weighted averaging over different simulations we were able to correctly correlate calculated binding free energies of (6*R*)- and (6*S*)-α-ionone binding to the experimentally determined data for M01 A82W. However, the low occurrence of the (6*S*)-α-ionone conformation in the substrate reference simulation in M11 L437N (Figure 7A) prohibited a similar match between calculated and experimentally determined binding free energy differences for this mutant. For the products we were able to reproduce experimental trends in free energies of binding, showing a lower binding affinity with respect to the system's reference state of the *trans*-3-OH-α-ionone products for M01 A82W and of the *trans*-(6*S*)-α-ionone and *cis*-(6*R*)-α-ionone hydroxylated products for M11 L437N.

CONCLUSION

Stereoselective hydroxylation of α-ionones by engineered Cytochrome P450 BM3 mutants has been studied using the one-step perturbation approach from an adequately chosen reference state. The Hamiltonian for the reference state was optimized free in solution by lowering force constants for several force field terms describing the substrate, leading to sufficient transitions between the two enantiomeric states. The optimized reference state model was successfully applied to the ligand in complex with CYP450 BM3 mutant M01 A82W to correctly estimate the relative free energy of binding of the substrate enantiomers and predict the observed trends in trans hydroxylation in accordance with experimentally determined data. This optimized model could also be applied in TI calculations, in which (6*R*)-α-ionone was transformed into (6*S*)-α-ionone via a modified flat intermediate state.

Applying the same approach to the binding of α-ionone stereoisomers to a second CYP450 BM3 mutant (M11 L437N), the experimental binding affinities for the two enantiomeric substrates were 6 kJ mol^{-1} off from experiment. This is because too few stereoinversions of the C6 stereocenter were observed in the substrate reference state simulations. Convergence of the calculated free energies of binding to M11 L437N may require longer simulations to allow for the breaking and formation of different ligand−protein hydrogen bonds in the active site. In the simulations of the product reference state, however, more inversions of the stereocenters were observed and predictions of the free energies of the four possible hydroxylation products were found to be in line with experimentally observed trends.

In conclusion, this study shows that free energy calculations can give insight into the stereoselective hydroxylation of α-ionones by engineered Cytochrome P450 BM3 mutants and that OSP offers an elegant way to calculate free energy differences between enantiomeric (or diastereomeric) compounds, possibly predicting formation of novel (hydroxylated) products or playing a supportive role in the rational design of new CYP450 BM3 mutants.

ASSOCIATED CONTENT

Supporting Information

Building block of the reference state as used in the one-step perturbation simulations for the product state. This material is available free of charge via the Internet at http://pubs.acs.org.

AUTHOR INFORMATION

Corresponding Author

*E-mail chris.oostenbrink@boku.ac.at.

Notes

The authors declare no competing financial interest.

ACKNOWLEDGMENTS

Financial support from Grant No. LS08-QM3 of the Vienna Science and Technology Fund (WWTF; S.d.B., C.O.), Grant No. 260408 of the European Research Council (ERC, C.O.) and VENI grant 700.59.406 of the Netherlands Organisation for Scientific Research (NWO, D.P.G.) is gratefully acknowledged.

REFERENCES

(1) Winterhalter, P.; Rouseff, R. *Carotenoid-derived aroma compounds*; American Chemical Society: Washington, DC, 2002; Vol. *802*.

(2) Withers, S. T.; Keasling, J. D. Biosynthesis and engineering of small molecules. *Appl. Microbiol. Biotechnol.* **2007**, *73*, 980−990.

(3) Brenna, E.; Fuganti, C.; Serra, S.; Kraft, P. Optically active ionones and derivates: Preparation and olfactory properties. *Eur. J. Org. Chem.* **2002**, *33*, 967−978.

(4) Brenna, E.; Fuganti, C.; Gatti, F. G.; Serra, S. Biocatalytic methods for the synthesis of enantioenriched odor active compounds. *Chem. Rev.* **2011**, *111*, 4036−4072.

(5) Eschenmoser, W.; Uevelhart, P.; Eugster, C. H. Synthesis and structure of of the enantiomeric 6-hydroxy-α-ionone and cis- and trans-5, 6-dihydroxy-5, 6-dihydro-β-ionone. *Helv. Chim. Acta* **1981**, *64*, 2681−2690.

(6) Duetz, W. A.; Bouwmeester, H.; van Beilen, J. B.; Witholt, B. Biotransformation of limonene by bacteria, fungi, yeast and plants. *Appl. Microbiol. Biotechnol.* **2003**, *61*, 269−277.

(7) Bicas, J. L.; Dionisio, A. P.; Pastore, G. M. Bio-oxidation of terpenes: an approach for the flavor industry. *Chem. Rev.* **2009**, *109*, 4518−4531.

(8) Torres Pazmino, W. E.; Winkler, M.; Glieder, A.; Fraaije, M. W. Monooxygenases as biocatalysts: Classification, mechanistic aspects and biotechnological applications. *J. Biotechnol.* **2010**, *146*, 9−24.

(9) Lutz-Wahl, S.; Fischer, P.; Schmidt-Dannert, C.; Wohlleben, W.; Hauer, B.; Schmid, R. D. Stereo- and regioselective hydroxylation of α-ionone by *Streptomyces* strains. *Appl. Environ. Microbiol.* **1998**, *64*, 3878−3881.

(10) Bernhardt, R. Cytochrome P450s as versatile biocatalysts. *J. Biotechnol.* **2006**, *124*, 128−145.

(11) Girhard, M.; Klaus, T.; Khatri, Y.; Bernhardt, R.; Urlacher, V. B. Characterization of the versatile monooxygenase CYP109B1 from *Bacillus subtilis*. *Appl. Microbiol. Biotechnol.* **2010**, *87*, 595−607.

(12) Girhard, M.; Machida, K.; Itoh, M.; Schmid, R. D.; Arisawa, A.; Urlacher, V. B. Regioselective biooxidation of (+)-valencene by recombinant *E. coli* expressing CYP109B1 from *Bacillus subtilis* in a two-liquid-phase system. *Microb. Cell. Fact.* **2009**, *10*, 8−36.

(13) Khatri, Y.; Girhard, M.; Romankiewicz, A.; Ringle, M.; Hannemann, F.; Urlacher, V. B.; Hutter, M. C.; Bernhardt, R. Regioselective hydroxylation of norisoprenoids by CYP109D1 from *Sorangium cellulosum* So ce56. *Appl. Microbiol. Biotechnol.* **2010**, *88*, 485−495.

(14) Ly, T. T. B.; Khatri, Y.; Zapp, J.; Hutter, M. C.; Bernhardt, R. CYP264B1 from *Sorangium cellulosum* So ce56: a fascinating norisoprenoid and sesquiterpene hydroxylase. *Appl. Microbiol. Biotechnol.* **2012**, *95*, 123−133.

(15) Guengerich, F. P. A malleable catalyst dominates the metabolism of drugs. *Proc. Natl. Acad. Sci.* **2006**, *103* (37), 13565−13566.

(16) Urlacher, V. B.; Lutz-Wahl, S.; Schmid, R. D. Microbiol P450 enzymes in biotechnology. *Appl. Microbiol. Biotechnol.* **2004**, *64*, 317−325.

(17) Urlacher, V. B.; Makhsumkhanov, A.; Schmid, R. D. Biotransformation of beta-ionone by engineered cytochrome P450 BM-3. *Appl. Microbiol. Biotechnol.* **2006**, *70*, 53−59.

(18) Appel, D.; Lutz-Wahl, S.; Fischer, P.; Schwaneberg, U.; Schmid, R. D. A P450 BM-3 mutant hydroxylates alkanes, cycloalkanes, arenes and heteroarenes. *J. Biotechnol.* **2001**, *88*, 167−171.

(19) Venkataraman, H.; de Beer, S. B. A.; Geerke, D. P.; Vermeulen, N. P. E.; Commandeur, J. N. M. Regio- and stereoselective hydroxylation of optically active α-ionone enantiomers by engineered cytochrome P450 BM3 mutants. *Adv. Synth. Catal.* **2012**, accepted, DOI: 10.1002/adsc.201200067.

(20) Stjernschantz, E.; Marelius, J.; Medina, C.; Jacobsson, M.; Vermeulen, N. P. E.; Oostenbrink, C. Are automated molecular dynamics simulations and binding free energy calculations realistic tools in lead optimization? An evaluation of the Linear Interaction Energy (LIE) method. *J. Chem. Inf. Model.* **2006**, *46*, 1972−1983.

(21) Foloppe, N.; Hubbard, R. Towards predictive ligand design with free-energy based computational methods? *Curr. Med. Chem.* **2006**, *13* (29), 3583−3608.

(22) McQuarrie, D. A. *Statistical mechanics*; University Science Books: Sausalito, CA, 2000.
(23) de Ruiter, A.; Oostenbrink, C. Free energy calculations of protein-ligand interactions. *Curr. Opin. Chem. Biol.* **2011**, *15*, 547−552.
(24) Christ, C. D.; Mark, A. E.; van Gunsteren, W. F. Basic ingredients of free energy calculations: a review. *J. Comput. Chem.* **2010**, *31*, 1569−1582.
(25) Tembe, B. L.; McCammon, J. A. Ligand - Receptor Interactions. *Comput. Chem.* **1984**, *8* (4), 281−283.
(26) Kollman, P. A. Free energy calculations: applications to chemical and biochemical phenomena. *Chem. Rev.* **1993**, *93*, 2395−2417.
(27) Zwanzig, R. W. High-temperature equation of state by a perturbation method. I. Nonpolar gases. *J. Chem. Phys.* **1954**, *22*, 1420−1426.
(28) Beveridge, D. L.; DiCapua, F. M. Free energy via molecular simulation: Applications to chemical and biomolecular systems. *Annu. Rev. Biophys. Biol.* **1989**, *18*, 431−492.
(29) Liu, H.; Mark, A. E.; van Gunsteren, W. F. Estimating the Relative Free Energy of Different Molecular States with Respect to a Single Reference State. *J. Phys. Chem.* **1996**, *100* (22), 9485−9494.
(30) Schäfer, H.; van Gunsteren, W. F.; Mark, A. E. Estimating relative free energies from a single ensemble: Hydration free energies. *J. Comput. Chem.* **1999**, *20* (15), 1604−1617.
(31) Kirkwood, J. G. Statistical mechanics of fluid mixtures. *J. Chem. Phys.* **1935**, *3* (5), 300−313.
(32) Riniker, S.; Christ, C. D.; Hansen, H. S.; Huenenberger, P. H.; Oostenbrink, C.; Steiner, D.; van Gunsteren, W. F. Calculation of relative free energies for ligand-protein binding, solvation, and conformational transitions using the GROMOS software. *J. Phys. Chem. B* **2011**, *115*, 13570−13577.
(33) Zhou, Y.; Oostenbrink, C.; van Gunsteren, W. F.; Hagen, W. R.; de Leeuw, S. W.; Jongejan, J. A. Relative stability of homochiral and heterochiral dialanine peptides. Effects of perturbation pathways and force-field parameters on free energy calculations. *Mol. Phys.* **2005**, *103*, 1961−1969.
(34) Oostenbrink, C. Free energy calculations from one-step perturbations. In *Computational drug discovery and design*; Baron, R., Ed.; Humana Press: New York, 2012; Vol. *819*, pp 487−499.
(35) Schmid, N.; Christ, C. D.; Christen, M.; Eichenberger, A. P.; van Gunsteren, W. F. Architecture, implementation and parallelisation of the GROMOS software for biomolecular simulation. *Comput. Phys. Commun.* **2012**, *183*, 890−903.
(36) Lins, R. D.; Hünenberger, P. H. A new GROMOS force field for hexopyranose-based carbohydrates. *J. Comput. Chem.* **2005**, *26*, 1400−1412.
(37) *Molecular Operating Environment (MOE)*; Chemical Computing Group Inc.: Montreal, Quebec, Canada.
(38) Berendsen, H. J. C.; Postma, J. P. M.; van Gunsteren, W. F.; Hermans, J. Interaction models for water in relation to protein hydration. In *Intermolecular Forces*; Pullman, B., Ed.; Reidel: Dordrecht, The Netherlands, 1981; pp 331−342.
(39) Ryckaert, J.-P.; Ciccotti, G.; Berendsen, H. J. C. Numerical integration of cartesian equations of motion of a system with constraints: Molecular dynamics of n-alkanes. *J. Comput. Phys.* **1977**, *23* (3), 327−341.
(40) Berendsen, H. J. C.; Postma, J. P. M.; van Gunsteren, W. F.; DiNola, A.; Haak, J. R. Molecular-dynamics with coupling to an external bath. *J. Chem. Phys.* **1984**, *81* (8), 3684−3690.
(41) Tironi, I. G.; Sperb, R.; Smith, P. E.; van Gunsteren, W. F. A generalized reaction field method for molecular-dynamics simulations. *J. Chem. Phys.* **1995**, *102* (13), 5451−5459.
(42) Heinz, T. N.; van Gunsteren, W. F.; Huenenberger, P. H. Comparison of four methods to compute the dielectric permittivity of liquids from molecular dynamics simulations. *J. Chem. Phys.* **2001**, *115*, 1125−1137.
(43) Jarzynski, C. Nonequilibrium equality for free energy differences. *Phys. Rev. Lett.* **1997**, *78*, 2690−2693.
(44) Oostenbrink, C.; van Gunsteren, W. F. Free energies of binding of polychlorinated biphenyls to the estrogen receptor from a single simulation. *Proteins* **2004**, *54*, 237−246.
(45) Stjernschantz, E.; Oostenbrink, C. Improved ligand-protein binding affinity predicitons using multiple binding modes. *Biophys. J.* **2010**, *98*, 2682−2691.
(46) Marcus, R. A. Chemical and electrochemical electron-transfer theory. *Annu. Rev. Phys. Chem.* **1964**, *15*, 155−196.
(47) Daura, X.; van Gunsteren, W. F.; Mark, A. E. Folding-unfolding thermodynamics of a β-heptapeptide from equilibrium simulations. *Proteins* **1999**, *34*, 269−280.